Acta Crystallographica Section B
Structural Science
ISSN 0108-7681

Electron density of $KNiF_3$: analysis of the atomic interactions

Vladimir Tsirelson,[a]* Yury Ivanov,[a] Elizabeth Zhurova,[b]† Vladimir Zhurov[c] and Kiyoaki Tanaka[b]

[a]Mendeleev University of Chemical Technology, Moscow 125047, Russia, [b]Nagoya Institute of Technology, Gokiso-cho, Showa-ku, Nagoya 466, Japan, and [c]Karpov Institute of Physical Chemistry, Vorontsovo pole 10, 103064 Moscow, Russia

† Also at CREST, Japanese Science and Technology Corporation.

Correspondence e-mail: tsirel@muctr.edu.ru

Received 2 September 1999
Accepted 29 November 1999

The topological analysis of the electron density in the perovskite $KNiF_3$, potassium nickel trifluoride, based on the accurate X-ray diffraction data, has been performed. The topological picture of the atomic interactions differs from that resulting from the classic crystal chemistry consideration. The shapes of atoms in $KNiF_3$ defined by zero-flux surfaces in the electron density are, in general, far from spherical. At the same time, their asphericity in the close-packed layer is very small. The topological coordination numbers of K and Ni are the same as the geometrical ones, whereas topological coordination for the F atom (6) differs from the geometrical value. The latter results from a specific shape of the Ni-atom basin preventing the bond-path formation between F atoms in the same atomic close-packed layer, in spite of the fact that the closest F—F distance is the same as K—F. Judging by the electron density value and curvature at the bond critical points, the K—F interaction in $KNiF_3$ can be considered ionic, while the Ni—F bond belongs to the polar covalent type. No correlation of the topological ionic radii with crystal or ionic radii was found in $KNiF_3$. Critical points in the electrostatic potential have also been studied.

1. Introduction

The electron density (ED), $\rho(\mathbf{r})$, defines, in principle, both the structure and all ground-state properties of multi-electron systems (Hohenberg & Kohn, 1964). To study these characteristics, it is necessary, first of all, to obtain an accurate ED and to develop the theoretical methods to extract the information from it. The topological theory (Bader, 1990) allows, in particular, quantitative structural information to be obtained from the ED. This theory is based on quantum mechanics and describes the main features of the $\rho(\mathbf{r})$ in terms of its gradient vector field, $\nabla\rho(\mathbf{r})$, critical points (CP) positions, $\mathbf{r}_c$, and ED curvature in each point $\mathbf{r}$. The CP, the point at which $\nabla\rho(\mathbf{r}_c) = 0$, is determined by its rank, λ_i, the number of non-zero eigenvalues of the Hessian (or curvature) matrix at $\mathbf{r}_c$, and signature, the sum of the algebraic signs of λ_i. The ED exhibits four kinds of non-degenerate CPs of rank 3: maxima (3,−3), saddle points (3,−1) and (3,+1) and minima (3,+3). They correspond to nuclear positions, bonds, rings and cages in the body of multi-electron multi-nuclear systems. All types of CPs are present in the crystals, their type and number fulfil the Poincare–Hopf–Morse relation (Morse & Cairns, 1969; Bader, 1990) and their positions are restricted by the space-group symmetry (Johnson, 1977; Zou & Bader, 1994; Martin Pendas *et al.*, 1997). Three Hessian eigenvalues, principal curvatures $\lambda_1 \leq \lambda_2 \leq \lambda_3$, characterize the ED curvatures in the CP along the corresponding mutually orthogonal directions.

© 2000 International Union of Crystallography
Printed in Great Britain – all rights reserved

In the $\nabla\rho(\mathbf{r})$ field, there are pairs of gradient lines originated at a (3,−1) CP and terminated at two neighbouring nuclei. They are determined by the eigenvector corresponding to a single positive eigenvalue of Hessian λ_3 at this point and they form the atomic interaction lines along which the ED decreases for any lateral displacements. This line, when in an equilibrium system, is termed a bond path and the associated (3,−1) point is termed a bond CP. Every bond path is mirrored by a line of maximally negative potential energy density connecting the same nuclei (Bader, 1998). The network of the bond paths linking neighbouring nuclei defines a molecular graph, its form being invariant to the nuclear vibrations in a stable system.

The nuclei of neighbouring atoms in any crystal and molecular system are separated in the $\nabla\rho(\mathbf{r})$ field by surfaces of zero flux, defined by the gradient lines terminated at the bond CP. All properties of such topological atoms are defined by quantum mechanics: a principle of stationary action, the Hohenberg–Kohn and virial theorems are valid for topological atoms (Bader, 1990, 1994).

A significant aspect of the topological theory deals with the spatial distribution of the Laplacian of the ED, $\nabla^2\rho(\mathbf{r})$, characterizing the concentration and depletion of electrons in each point of a system. The local potential energy, in the bonded systems, dominates in the points where $\nabla^2\rho(\mathbf{r}) < 0$. The sign of the Laplacian at the bond CP $\nabla^2\rho(\mathbf{r}_c) = \lambda_1 + \lambda_2 + \lambda_3$ is particularly interesting from the structural point of view: it depends on the relation between principal curvatures of the ED at $\mathbf{r}_c$ and, therefore, reflects the character of atomic interactions. The negative eigenvalues λ_1 and λ_2 in the bond CP correspond with the normal directions to the bond path and measure the degree of ED contraction toward this point; $\lambda_3 > 0$ measures the degree of ED contraction towards each of the neighbouring nuclei. If the electrons are locally concentrated in the bond CP, then ED is shared by both nuclei, a picture, which is typical for a covalent bond. If the positive curvature dominates in the bond CP, the electrons are concentrated in each of the atomic basins separately. Such closed-shell interactions are usually observed in the ionic and hydrogen bonds, as well as van der Waals interactions.

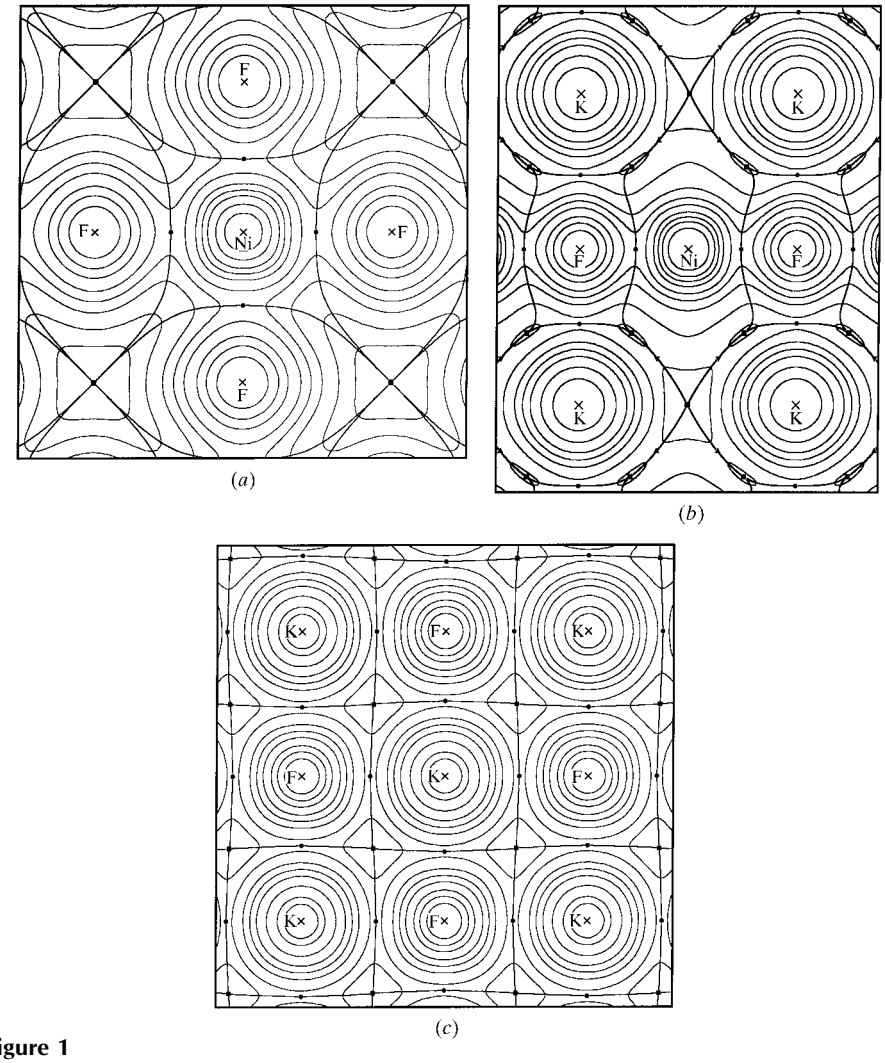

Figure 1
Model static electron density maps of $KNiF_3$ overlaid with interatomic zero-flux surfaces: (*a*) (100) plane; (*b*) (110) plane; (*c*) (200) plane. Critical points (3,−1), (3,+1) and (3,+3) are denoted by dots, triangles and squares, respectively; bond paths going through (3,−1) critical points did not appear.

Thus, topological theory considers a crystal (molecule) as a set of interacting atoms connected by bond paths, similar to classic crystal chemistry. In contrast to the latter, however, the former is based on quantum mechanics and provides a bridge between electron-density descriptions of crystals, and geometrical and energetic notions of the solid-state physics and chemistry.

It should be noted that topological theory was developed for the 'true' quantum mechanical electron density. After that it was applied to analysis of the ED reconstructed from precise X-ray diffraction data (Tsirelson & Ozerov, 1986; Lau *et al.*, 1986; Kapphahn *et al.*, 1988*a*,*b*; Lobanov *et al.*, 1988; Stewart, 1991; Destro *et al.*, 1991; Downs & Swope, 1992; Klooster *et al.*, 1992; Tsirelson *et al.*, 1995; Destro & Merati, 1995; Iversen *et al.*, 1995; Roversi *et al.*, 1996; McCormak *et al.*, 1996; Ivanov *et al.*, 1998; Koritsanszky *et al.*, 1998; Kapphahn, 1989; Tsirelson, 1993). The ED reconstruction from experiment is normally realised with some analytical structural model. Hence, the ED model suffers from insufficiently corrected systematic experimental errors (absorption, thermal diffuse and multiple scattering, extinction *etc.*) and restrictions such as limited resolution, incomplete thermal deconvolution as well as

from random and model errors (Tsirelson & Ozerov, 1996). That is why the model ED is only a homeomorphic image of the 'true' $\rho(\mathbf{r})$ derived from first principles, coinciding with $\rho(\mathbf{r})$ in some points and deviating in others. It is important, however (Kapphahn *et al.*, 1988*a*,*b*; Tsirelson, 1996), that the experimental ED exhibits the same set of critical points as 'true' $\rho(\mathbf{r})$ (the problems arising during a localization of the CP in low-density near-uniform areas were discussed by Tsirelson *et al.*, 1998). Thus, the ED reconstructed from the X-ray diffraction data can be used in the analysis of the atomic interactions in the crystals.

The aim of this work is the topological analysis of the experimental ED of cubic perovskite $KNiF_3$. We shall also present the description of the topological features of the electrostatic potential in this crystal.

Cubic perovskites contain one ABC_3 formula in the unit cell. The symmetry of the *A* and *B* atom positions is $m3m$, while the *C* atom is situated in the $4/mmm$ position. Classical crystal chemistry tells us that atom *A* is coordinated by 12 *C* atoms and atom *C* is coordinated by four *A* and eight other *C* atoms. *A* and *C* atoms together build a close-packed atomic layers, while the *B* atoms are sited in the octahedral holes. It is interesting to compare this geometrical consideration with a topological one. Theoretical analysis of the topological features of the ED in perovskites was given by Luana *et al.* (1997).

The deformation ED of $KNiF_3$ has been studied previously by Kijima *et al.* (1983), Maslen & Spadaccini (1989) and Ivanov *et al.* (1999), and is not presented in this paper.

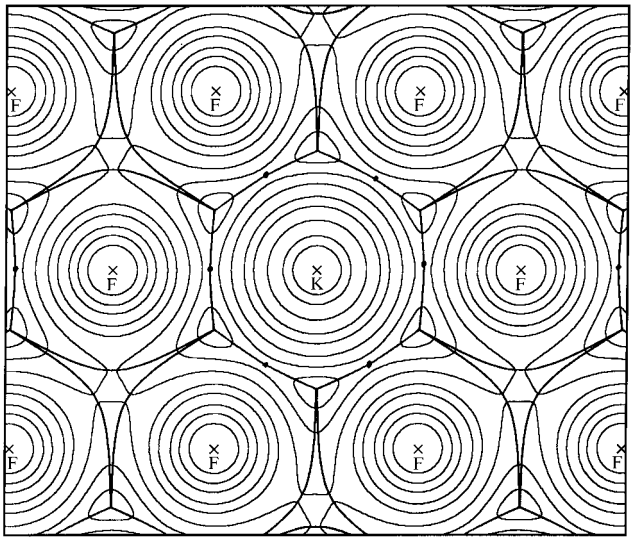

Figure 2
Model static electron density maps of $KNiF_3$ overlaid with interatomic zero-flux surfaces: (*a*) (111) plane; (*b*) (222) plane. For an explanation of the notation see caption to Fig. 1.

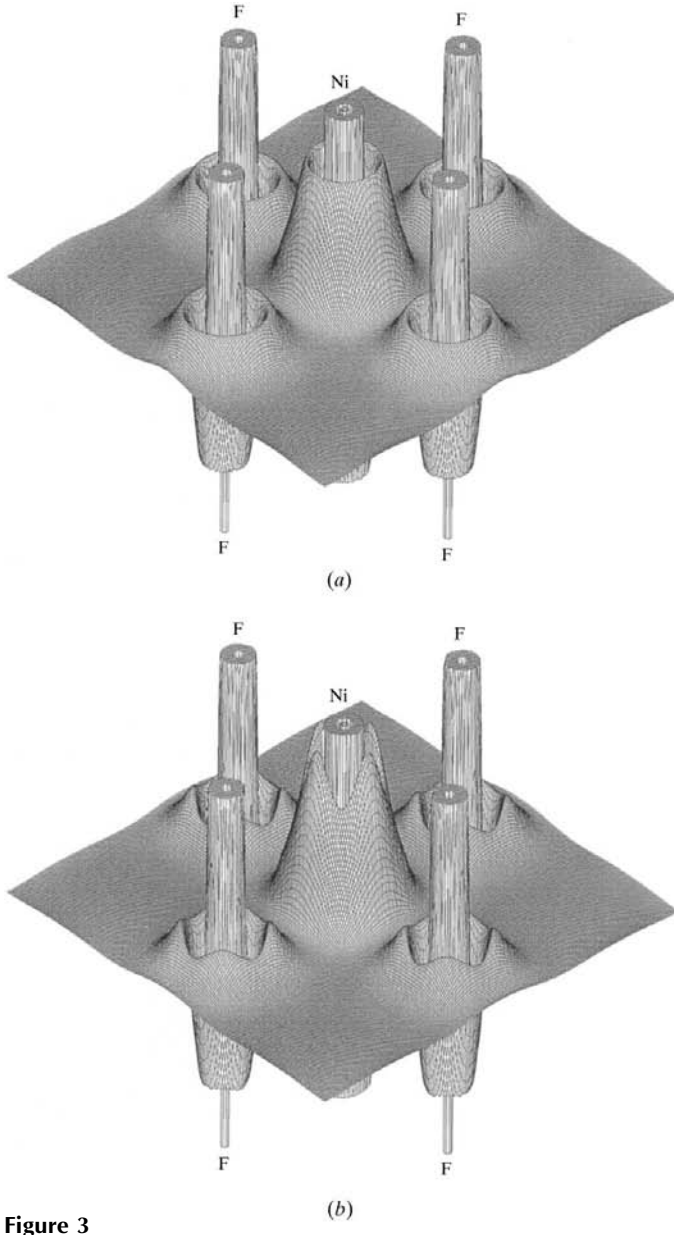

Figure 3
Laplacian of the electron density in the (100) plane of $KNiF_3$: (*a*) $\nabla^2\rho$ of the procrystal consisting of spherical atoms; (*b*) $\nabla^2\rho$ of the model electron density. To make the $+\nabla^2\rho$ features more distinct, the vertical scale appears to be nonlinear and truncated at 500 e Å^{-5}.

Table 1
Characteristics of the critical points in $KNiF_3$.

Experimental results are given in the first line and procrystal results in the second.

Critical point position	X	Y	Z	$\rho(\mathbf{r}_{cp})$ (e Å^{-3})	$\nabla^2\rho(\mathbf{r}_{cp})$ (e Å^{-5})	λ_1 (e Å^{-5})	λ_2 (e Å^{-5})	λ_3 (e Å^{-5})	Type of critical point
$(x,0,0)$	0.2435	0	0	0.50 (2)	7.08 (19)	−2.45	−2.45	11.98	(3,−1)
	0.2537	0	0	0.47	9.08	−2.19	−2.19	13.47	
$(\frac{1}{2},x,x)$	0.5	0.2395	0.2395	0.07 (1)	1.41 (4)	−0.26	−0.08	1.75	(3,−1)
	0.5	0.2382	0.2382	0.08	1.29	−0.21	−0.16	1.65	
(x,y,y)	0.2510	0.2747	0.2747	0.04(1)	0.60(2)	−0.06	0.26	0.40	(3,+1)
	0.2394	0.2808	0.2808	0.06	0.58	−0.01	0.04	0.55	
$(0,\frac{1}{2},\frac{1}{2})$	0	0.5	0.5	0.02 (1)	0.28 (2)	0.08	0.08	0.12	(3,+3)
	0	0.5	0.5	0.03	0.17	0.05	0.05	0.07	
(x,x,x)	0.2666	0.2666	0.2666	0.04 (1)	0.59 (2)	0.03	0.03	0.53	(3,+3)
	0.2665	0.2665	0.2665	0.06	0.57	0.01	0.01	0.55	

2. Data treatment

For topological analysis we used a quasi-static electron density of $KNiF_3$ (a = 4.0108 Å) reconstructed by Ivanov *et al.* (1999) from very accurate four-circle X-ray diffractometer measurements at room temperature. Experimental data were corrected for multiple scattering, thermal diffuse scattering, absorption, extinction and anomalous scattering. The ED was approximated by the Hansen & Coppens (1978) multipole model, using an expansion up to hexadecupoles. This model was fitted to the experimental structure factors, taking into account an anharmonicity of the atomic displacements (R = 0.0038, wR = 0.0036, S = 1.22). Experimental details and details of the refinement are described by Ivanov *et al.* (1999).

The (static) ED and Laplacian of the ED were calculated from the multipole parameters derived from the experimental structure factors. Maps of these functions in the most important sections of $KNiF_3$ are presented in Figs. 1–3. We have also found all CPs in the ED and calculated the curvatures of the ED, λ_i, in these points. These characteristics and those for a procrystal consisting of the spherical atoms are listed in Table 1.

We have also studied the topological features of the electrostatic potential, $\varphi(\mathbf{r})$, in $KNiF_3$. This value is connected with a charge density $\sigma(r) = \sum_a Z_a\delta(r - R_a) - \rho(r)$ by the relation

$$\varphi(\mathbf{r}) = \sum_a \left\{ Z_a/(|\mathbf{r} - R_a|) - \int_{-\infty}^{\infty} \{\rho(\mathbf{r}')/|\mathbf{r} - \mathbf{r}'|\}\mathrm{d}\mathbf{r}' \right\}.$$

Here Z_a is the nuclear charge of atom a and $\rho(\mathbf{r})$ is the electron density approximated by the multipole model. The electrostatic potential maps, with superimposed (3,−1) CPs, are given in Fig. 4.

The topological analysis of $KNiF_3$ was performed with the *XPRO*98 program (Ivanov *et al.*, 1997).

3. Discussion

The topological analysis of the model experimental ED for $KNiF_3$ shows the following features. Six (3,−1) CPs are situated on Ni—F lines (internuclear distance 2.0054 Å) and 12 are on K—F lines (2.8361 Å). Thus, the geometrical and topological coordination numbers of Ni and K atoms are the same: 6 and 12, respectively. The bond paths connect each F atom with two Ni and four K atoms (see Fig. 1). However, in spite of the fact that the closest F—F distance, 2.8361 Å, is the same as K—F, the F atom does not form the bond paths with six other F atoms surrounding it in the same close-packed layer (Fig. 2*b*). Hence, the topological coordination number of the F atom is 6, which is different to the geometrical one.

The character of the atomic interactions between Ni and F atoms and between K and F atoms is particularly interesting in view of these findings. Positive values of the Laplacian of the ED in the (3,−1) CPs indicate, according to Bader (1990), that closed-shell atomic interactions take place in both these cases. This conclusion agrees with the distribution of the atomic charges $K^{+1}Ni^{+0.29}F_3^{-0.43}$ found by Ivanov *et al.* (1999) with a multipole model. At the same time, the ED value in the Ni—F bond CP is seven times more than that in K—F, reflecting a significant covalent component of the Ni—F interaction (Table 1). ED curvatures λ_1 and λ_2 in the Ni—F bond are also significantly larger, demonstrating a bigger ED contraction to the bond path. Tsirelson (1999) has recently considered the molecules and crystals with different types of atomic interactions and found that the typical ED value in ionic bond CPs ranges from 0.07 to 0.25 e Å^{-3} with $|\lambda_1|/\lambda_3 \simeq 0.14$. Thus, the K—F interaction in $KNiF_3$, whose characteristics correspond to these values, can be considered as ionic, while the Ni—F bond is an intermediate (according to Bader & Essen, 1984*a*) or polar covalent bond.

The shapes of atoms in $KNiF_3$, defined by zero-flux surfaces in the $\nabla\rho(\mathbf{r})$ field, are seen in Figs. 1 and 2. They are, in general, non-spherical to a different extent. In particular, easy polarized F^- ions are compressed along the Ni—F line and significantly extended perpendicular to it. It can be concluded that the specific shape of the ED basin of the Ni atom prevents the formation of the F—F bond path. Martin Pendas *et al.* (1997) found the same shape of the B^{2+} ion basin in a series of perovskites with the same set of critical points as $KNiF_3$.

The ratios $R(\mathrm{Ni})/R(\mathrm{F} \rightarrow \mathrm{Ni})$ = 0.95 and $R(\mathrm{K})/R(\mathrm{F} \rightarrow \mathrm{K})$ = 1.05, where $R(\mathrm{F} \rightarrow \mathrm{Ni})$, $R(\mathrm{K})$ and $R(\mathrm{Ni})$ are distances from the corresponding nuclei to the bond CPs (directional topological ionic radii), are, according to Martin Pendas *et al.* (1997), typical for cubic perovskites with the same set of critical points as $KNiF_3$. At the same time, no correlation of the topological ionic radii with crystal or ionic (Shannon, 1976) radii was found in $KNiF_3$ (see Tables 2 and 3).

Table 2
Topological atomic radii (Å) for crystals and procrystals of $KNiF_3$ and empirical crystal and ionic radii according to Shannon (1976).

Empirical: Geometrical coordination number is indicated in brackets.

Atom	Topological (crystal)	Topological (procrystal)	Empirical CR	Empirical IR	
K R(K → F)	1.478	1.486	1.78	1.64	{12}
Ni	0.977	1.017	0.83	0.69	{6}
R(F → K)	1.358	1.351			
F			1.145	1.285	{2}
R(F → Ni)	1.028	0.988			

Table 3
Topological atomic radii (Å) for $KNiF_3$ derived from the electrostatic potential.

	Atom	Topological ESP radius
K	R(K → F)	1.78
	R(K → Ni)	1.78
	R(K → K)	2.02 (= a/2)
Ni	Ni → K	1.69
	Ni → F	1.18
F	R(F → K)	1.06
	R(F → Ni)	0.83

The depletion of the ED, manifesting itself by $\nabla^2\rho > 0$, occurs in a substantial portion of the internuclear space of $KNiF_3$ (Fig. 3): the ED features are concentrated mainly around ions. The map of the Laplacian reveals the quantum electron shells; the $\nabla^2\rho$ distribution does not allow us to resolve the outer 3d and 4s valence electron shells of Ni. Along the bond paths, the Ni—F interaction enhances the electron depletion in the outer Ni-atom valence shells and diminishes it in the L electron shell of the F atom. It reflects the charge transfer from Ni to F. Simultaneously, electron depletion in the outer Ni-atom valence shells along the [110] (and [111]) direction is smaller than that in the free atom: it corresponds to some concentration of the electrons on t_{2g} orbitals of the Ni atom found by Ivanov *et al.* (1999).

To have a look at the topological features of the atomic close packing in the $KNiF_3$ crystal, consider the ED in the (111) and (222) planes of the $KNiF_3$ unit cell. Fig. 2(*a*) presents a plane containing only Ni atoms, occupying the octahedral holes between K and F atoms, while the plane in Fig. 2(*b*) goes through the K—F close-packed layer. The pattern of atomic zero-flux boundaries reveals a behaviour, which differs from that resulting from the classical close-packing concept. The latter implies that all atoms in the K—F close-packed layer make contact with each other, while topological analysis shows that the ED basins of the F atoms are separated by the Ni atom basins (Fig. 1*a*): therefore, only K—F interactions take place in this plane. At the same time, all atoms in the section discussed can be well approximated by spheres, in agreement with the main assumption of the close-packing concept. Deviation of the atomic ED from sphericity close to atomic boundaries in the (222) plane is only noticeable starting from the ED of 0.17 e Å^{-3} for the F atom and 0.07 e Å^{-3} for the K atom. Note that the F and K atoms are almost spherical in the (200) plane also (Fig. 1*c*).

ED basins of the Ni atoms are well separated in the (222) plane (Fig. 2*a*). Asphericity of the Ni atoms in this plane manifests itself starting with the ED value of 0.12 e Å^{-3}.

It is worth noting that the topological characteristics of the $KNiF_3$

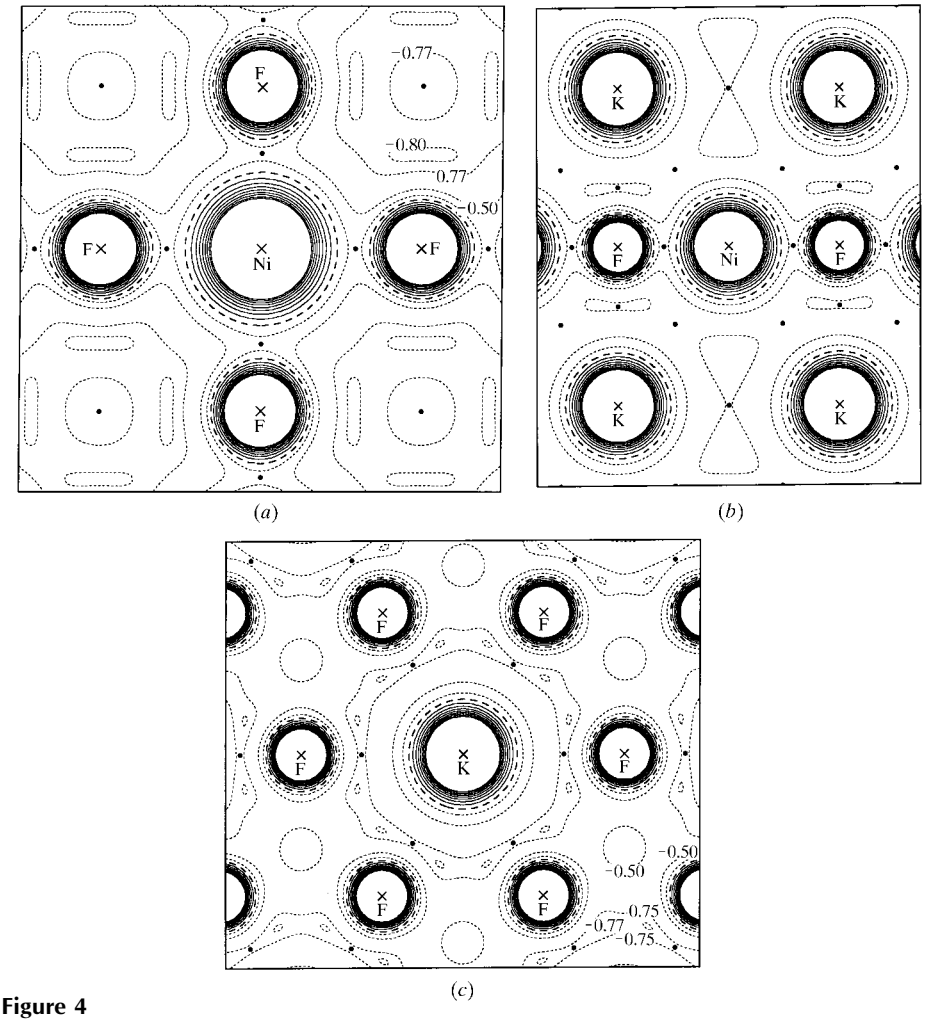

Figure 4
Maps of the electrostatic potential in $KNiF_3$: (*a*) (100) plane; (*b*) (110) plane; (*c*) (222) plane. Contour intervals are 0.25 e Å^{-1}, excluding lines connected with small ESP features, which are specified in the figure. Positive contours are solid. The mean inner ESP was chosen in such a way that the average ESP over a unit cell is zero.

procrystal (Table 1) exhibit the same pattern as the real crystals, their values being in reasonable quantitative agreement. The maximal difference between the (3,−1) CP positions on the Ni—F and K—F lines in the crystal and procrystal EDs is only 0.04 Å. A similar observation was previously noted for some binary crystals and silica polymorphs by Gibbs *et al.* (1992), and for the rock-salt crystals by Tsirelson *et al.* (1998). Thus, the topological analysis of a procrystal provides an approximate *a priori* estimate of the structural features of real crystals (at least, for first-neighbour interactions), in addition to energy characteristics, as suggested by Spackman & Maslen (1986) and Trefry *et al.* (1987). Of course, we should keep in the mind that the procrystal is an unstable nonbounded system, which does not obey the variational and Pauli exclusion principles and the virial theorem, and has a different $\nabla^2\rho(\mathbf{r})$ distribution (Fig. 3).

The (3,−1) CPs in the electrostatic potential (ESP) were found on Ni—F, K—F, Ni—K and K—K lines (Fig. 4). The first two correspond to the bond CP in the ED, while the other two appeared on the same points, where the minimum in the ED exists. Simultaneously, other types of CPs are observed in the vicinity of the F atoms (see Figs. 4*a* and *c*). Thus, the ESP and the ED fields have different sets of critical points.

The origin of the topological ESP picture observed has the following explanation. Nuclei are not real maxima, or (3,−3) CP, in the ESP scalar field. However, the behaviour of the ESP close to the nuclei is indistinguishable from that for true (3,−3) critical points (Tal *et al.*, 1980). Therefore, nuclear positions can be considered as maxima in the ESP field, with no other strict local maxima in the ESP (Pathak & Gadre, 1990). Now take into account that the ESP distribution, unlike sign-permanent ED, has a specificity resulting from the different properties of positive and negative mononuclear ions (Weinstein *et al.*, 1975; Sen & Politzer, 1989). The ESP of positive ions (and neutral atoms) is always positive and monotonically decays approaching zero. The ESP of negative ions is positive only within some sphere: it also monotonically decays, going through zero, and attains a unique (negative) minimum at some distance from the nuclei (Fig. 5). It is the superposition of all ionic ESP at each point that defines the ESP distribution, the actual sign of the inner-crystal ESP depending on the choice of mean inner ESP (O'Keeffe & Spence, 1994).

The (3,−1) CP in the ESP of the multi-nuclear systems will occur on the lines connecting properly placed maxima, including pairs of non-interacting (in the Bader's sense) atoms. This is the case in $KNiF_3$, even on the K—K line that connects quite distant ions. The features of the ESP behind the interatomic lines depend on both the crystal structure and the mutual sizes, and the charges of the positive and negative ions. This is clearly seen from the inspection of the ESP distribution in $KNiF_3$ close to the F atoms around the (3,+3) CP in the ED (Figs. 4*a* and *c*).

Similar to the $\nabla\rho(\mathbf{r})$ field, the nuclei of neighbouring atoms in any crystal (and molecule) are separated in the $\nabla\varphi(\mathbf{r})$ field by zero-flux surfaces S_i defined by the gradient lines terminated at the (3,−1) CP

$$\mathbf{E}(\mathbf{r})\cdot\mathbf{n}(\mathbf{r}) = -\nabla\varphi(\mathbf{r})\cdot\mathbf{n}(\mathbf{r}) = 0 \quad \forall\mathbf{r}\in S_i(\mathbf{r}).$$

[$\mathbf{n}(\mathbf{r})$ is a vector normal to the surface at $\mathbf{r}$]. However, in contrast to the $\nabla\rho(\mathbf{r})$ field, these surfaces define the atomic basins, inside which the nuclear charges are completely screened by the electronic cloud. In other words, the ESP

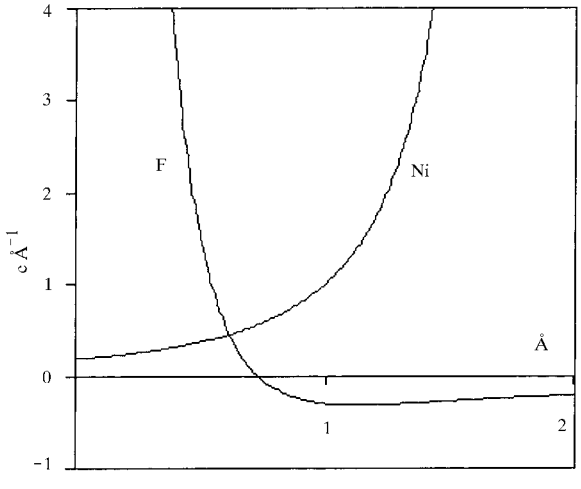

Figure 5
Superposition of the electrostatic potentials of F (x = 0) and Ni (x = 2.0054 Å) atoms calculated with experimentally determined atomic electron valence occupancies P_v = 9.77 and 7.42 and contraction/expansion parameters κ = 0.993 and 0.977 for Ni and F, respectively. The electrostatic potential at infinity was zero.

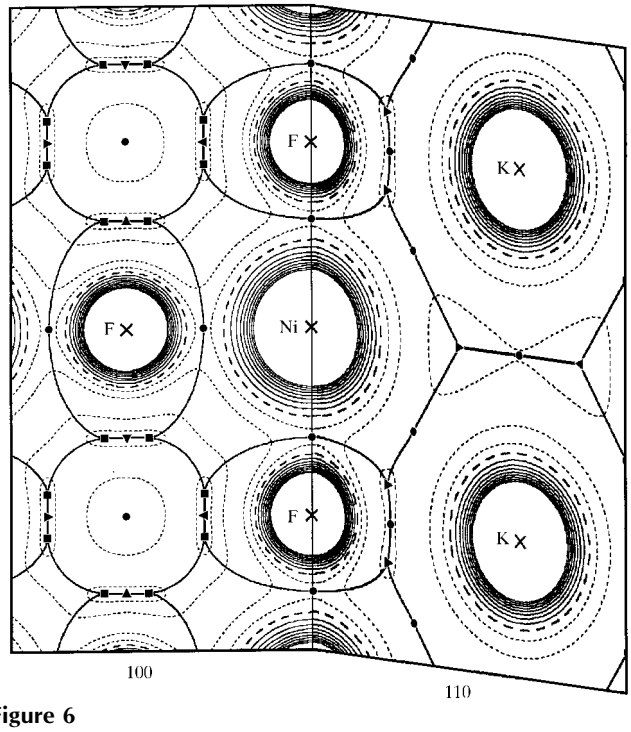

Figure 6
The 'patchwork' map of the electrostatic potential in $KNiF_3$ consisting of (100) and (110) planes overlaid with interatomic zero-flux surfaces in the $\nabla\varphi(\mathbf{r})$ field. Contour intervals are the same as in Fig. 4(*a*), positive contours are solid. Critical points (3,−1), (3,+1) and (3,+3) in the electrostatic potential are denoted by dots, triangles and squares, respectively.

atomic basins reveal the electrically neutral *bonded* pseudo-atoms. Comparison of the shapes of the latter (Fig. 6) with the shapes of the ED basins (Fig.1) helps to understand the role of the different factors in forming the crystal structure of $KNiF_3$.

Bader & Essen (1984*b*) have shown that, at equilibrium, the density of the total force exerted on an element of the ED at the point **r**, Ehrenfest (1927) force, depends on the two-electron density matrix. The ESP defines the electrostatic field at point **r**, $\mathbf{E}(\mathbf{r}) = -\nabla\varphi(\mathbf{r})$, and, therefore, defines the classical electrostatic (one-electron) component of this force. The CP in the ESP, excluding nuclear positions, are points where the electric field force exerted on the electron density is zero. That does mean that the only non-conservative quantum force determined by the correlation in the electron motion (including exchange) is effective in these points: only this force is balanced here by a momentum flux density (Bader & Essen, 1984*b*; Bader, 1998).

In conclusion, we would like to stress that the topological analysis of the electron density does result in a better scheme of atomic interactions in perovskites than classical crystal chemistry. This scheme is based on a limited number of well defined approximations and is consistent with quantum mechanics. The topological features of the electrostatic potential also carry valuable physical information about the crystal.

Authors thank Professor R. F. W. Bader for comments concerning the topological analysis of the electrostatic potential. Support of this work by the Japanese Ministry of Education, Science, Sports and Culture (grant # 09045034) is gratefully acknowledged.

References

Bader, R. F. W. (1990). *Atoms in Molecules – A Quantum Theory.* Oxford University Press.

Bader, R. F. W. (1994). *Phys. Rev. B*, **49**, 13348–13356.

Bader, R. F. W. (1998). *J. Phys. Chem. A*, **102**, 7314–7323.

Bader, R. F. W. & Essen, H. (1984*a*). *J. Chem. Phys.* **80**, 1943–1960.

Bader, R. F. W. & Essen, H. (1984*b*). *Local Density Approximation in Quantum Chemistry and Solid State Physics*, edited by J. P. Dahl & J. Avery, pp. 129–144. New York: Plenum Press.

Destro, R., Bianchi, R., Gatti, C. & Merati, F. (1991). *Chem. Phys. Lett.* **186**, 47–52.

Destro, R. & Merati, F. (1995). *Acta Cryst.* B**51**, 559–570.

Downs, J. W. & Swope, R. J. (1992). *J. Phys. Chem.* **96**, 4834–4840.

Ehrenfest, P. (1927). *Z. Phys.* **45**, 455–459.

Gibbs, G. V., Spackman, M. A. & Boisen, M. B. (1992). *Am. Mineral.* **77**, 741–750.

Hansen, N. K. & Coppens, P. (1978). *Acta Cryst.* A**34**, 909–921.

Hohenberg, P. & Kohn, W. (1964). *Phys. Rev. B*, **136**, 864–871.

Ivanov, Yu., Abramov, Yu. & Tsirelson, V. (1997). National Conference on Application of the X-ray, Neutrons and Electrons for Study of Materials. Abstracts. JINR, Dubna, p. 599.

Ivanov, Yu. V., Belokoneva, E. L., Hansen, N., Protas, J. & Tsirelson, V. G. (1998). *Acta Cryst.* B**54**, 774–781.

Ivanov, Yu. V., Zhurova, E. A., Zhurov, V. V., Tanaka, K. & Tsirelson, V. G. (1999). *Acta Cryst.* B**55**, 923–930.

Iversen, B. B., Larsen, F. K., Souhassou, M. &Takata, M. (1995). *Acta Cryst.* B**51**, 580–591.

Johnson, C. K. (1977). Am. Crystallogr. Assoc. Winter Meeting, Asilomar, Abstracts p. 30.

Kapphahn, M. (1989). PhD Thesis. Mendeleev University, Moscow.

Kapphahn, M., Tsirelson, V. G. & Ozerov, R. P. (1988*a*). *Dokl. Phys. Chem.* **303**, 1025–1028.

Kapphahn, M., Tsirelson, V. G. & Ozerov, R. P. (1988*b*). *Port. Phys.* **19**, 213–216.

Kijima, N., Tanaka, K. & Marumo, F. (1983). *Acta Cryst.* B**39**, 557–561.

Klooster, W. T., Swaminathan, S., Nanni, R. & Craven, B. M. (1992). *Acta Cryst.* B**48**, 217–227.

Koritsanszky, T., Flaig, R., Zobel, D., Krane, H.-G., Morgenroth, W. & Luger, P. (1998). *Science*, **279**, 356–358.

Lau, C. D. H., Bader, R. F. W., Hermansson, K. & Berkovich-Ellin, Z. (1986). *Chem. Scr.* **26**, 476.

Lobanov, N. N., Belokoneva, E. L. & Tsirelson, V. G. (1988). *Russ. J. Inorg. Chem.* **32**, 1740–1744.

Luana, V., Costales, A. & Martin Pendas, A. (1997). *Phys. Rev. B*, **55**, 4285–4297.

Maslen, T. & Spadaccini, N. (1989). *Acta Cryst.* B**45**, 45–52.

McCormak, K. L, Mallinson, P. R., Webster, B. C. & Yufit, D. S. (1996). *J. Chem. Soc. Faraday Trans.* **92**, 1709–1716.

Martin Pendas, A., Costales, A. & Luana, V. (1997). *Phys. Rev. B*, **55**, 4275–4284.

Morse, M. & Cairns, S. S. (1969). *Critical Point Theory in Global Analysis and Differential Geometry.* New York: Academic Press.

O'Keeffe, M. & Spence, J. C. H. (1994). *Acta Cryst.* A**50**, 33–50.

Pathak, R. K. & Gadre, S. R. (1990). *J. Chem. Phys.* **93**, 1770–1773.

Roversi, P., Barzaghi, M., Meratti, F. & Destro, R. (1996). *Can. J. Chem.* **74**, 1145–1161.

Sen, K. D. & Politzer, P. (1989). *J. Chem. Phys.* **90**, 4370–4372.

Shannon, R. D. (1976). *Acta Cryst.* A**32**, 451–467.

Spackman, M. A. & Maslen, E. N. (1986). *J. Phys. Chem.* **90**, 2020–2027.

Stewart, R. F. (1991). *NATO ASI Ser. B Phys.* **250**, 63–102.

Tal, Y., Bader, R. F. W. & Erkku, R. (1980). *Phys. Rev. A*, **21**, 1–11.

Trefry, M. G., Maslen, E. N. & Spackman, M. A. (1987). *J. Phys. C*, **20**, 19–27.

Tsirelson, V. G. (1993). *The Chemical Bond and Thermal Atomic Motion in Crystals.* Moscow: VINITI Publishers.

Tsirelson, V. G. (1996). *Can. J. Chem.* **74**, 1171–1180.

Tsirelson, V. G. (1999). XVIIIth Congress and General Assembly. 4–13 August 1999. Glasgow, Scotland. Abstract M13.OF.003, p. 207.

Tsirelson, V. G., Abramov, Yu. A., Zavodnik, V., Stash, A., Belokoneva, E. L., Stahn, J., Pietsch, U. & Feil, D. (1998). *Struct. Chem.* **9**, 249–254.

Tsirelson, V. G. & Ozerov, R. P. (1986). *Application of X-rays to the Study of Materials*, edited by T. I. Malinovsky, p. 103. Kishinev: Shtiintsa Publishers.

Tsirelson, V. G. & Ozerov, R. P. (1996). *Electron Density and Bonding in Crystals.* Bristol and Philadelphia: IOP.

Tsirelson, V. G., Zou, P. F., Tang, T.-H. & Bader, R. F. W. (1995). *Acta Cryst.* A**51**, 143–153.

Weinstein, H., Politzer, P. & Srebrenik, S. (1975). *Theor. Chim. Acta*, **38**, 159–164.

Zou, P. F. & Bader, R. F. W. (1994). *Acta Cryst.* A**50**, 714–725.